Journal of Catalysis **199,** 224–235 (2001)
doi:10.1006/jcat.2000.3158, available online at http://www.idealibrary.com on IDEAL®

# The Relation between Morphology and Hydrotreating Activity for Supported $MoS_2$ Particles

E. J. M. Hensen,[1] P. J. Kooyman,[2] Y. van der Meer,[3] A. M. van der Kraan,[3]
V. H. J. de Beer, J. A. R. van Veen, and R. A. van Santen

*Schuit Institute of Catalysis, Eindhoven University of Technology, P.O. Box 513, 5600 MB Eindhoven, The Netherlands*

Received August 8, 2000; revised December 8, 2000; accepted December 18, 2000; published online March 21, 2001

**Supported Mo–sulfide catalysts were structurally characterized by means of transmission electron microscopy (TEM), dynamic oxygen chemisorption (DOC), and EXAFS. The catalysts show the well-known $MoS_2$ slab structures with a multilayered morphology in the case of $Mo/SiO_2$ and Mo/ASA. The $MoS_2$ edge dispersion was evaluated from the TEM micrographs. While sulfidation of $Mo/Al_2O_3$ results in a highly dispersed, mostly single–layered $MoS_2$ phase, a decreased metal–support interaction (NTA addition) or use of supports with a lower metal–support interaction leads to a higher stacking degree concomitant with a loss in edge dispersion. Combined TEM and DOC results reveal that Mo/C has the highest $MoS_2$ dispersion. Reaction rate constants corrected for $MoS_2$ dispersion for hydrodesulfurization (HDS) and hydrogenation (HYD) of thiophene and dibenzothiophene and HYD of toluene were measured. In general, HYD rates increase with an increasing stacking degree attributed to a less hampered planar adsorption geometry of reactants on multilayered $MoS_2$. In contrast to the HDS rate constant of the small thiophene molecule, the DBT HDS rate constant is also strongly dependent on the stacking degree. It is concluded that perpendicular adsorption via sulfur is favored for HDS of thiophene, while in the DBT case a planar adsorption geometry is preferred. Carbon is the preferred support for the HYD of thiophene and toluene, most likely due to the large fraction of corner sites. A real support effect is also found for Mo/ASA, which exhibits low intrinsic HDS activities compensated by very high HYD activity. The present results indicate that the selectivities for hydrodesulfurization and hydrogenation can be fine-tuned by the morphology of the $MoS_2$ phase and the choice of support.** 

*Key Words:* **hydrotreating; $MoS_2$; morphology; dispersion; TEM; EXAFS; thiophene; dibenzothiophene; hydrodesulfurization; toluene; hydrogenation.**

## INTRODUCTION

Molybdenum-based hydrotreating catalysts make up the larger part of the catalytic materials used for hydrotreating of oil feedstock. Detailed structural information concerning these catalysts, which consist mostly of alumina-supported Co(Ni)-promoted $MoS_2$, is difficult to obtain because of their structural complexity. Both the highly dispersed nature of the active sulfide species and the diversity of species (e.g., "Co–Mo–S," $MoS_2$, $Co_9S_8$, and $CoAl_2O_4$ structures in alumina-supported CoMo sulfide) are complicating factors. Moreover, the particular sensitivity of this type of catalysts to reoxidation of the sulfide phase necessitates the use of *in situ* techniques. The study of supported unpromoted $MoS_2$ particles provides some reduction of this complexity and has been widely employed. In the sulfided state, alumina-supported Mo catalysts exhibit $MoS_2$ slabs building a layered structure (1). There are indications for at least two types of (Co)$MoS_2$ phases (2, 3), a type I phase with highly dispersed monolayer $MoS_2$ particles and a more active type II phase that is essentially fully sulfided and mostly characterized by lower dispersion and a higher stacking degree. EXAFS analyses show typical lengths of the $MoS_2$ structures of 1.0–1.5 nm both in supported $MoS_2$ and in its promoted counterparts (4, 5), while transmission electron microscopy (TEM) data show larger lateral sizes (6–8). Whereas EXAFS underestimates this parameter due to the absence of long-range ordering (1), the smallest $MoS_2$ particles may be too small to be seen by TEM (7). Shido and Prins (9) simulated EXAFS spectra to account for disorder in the $MoS_2$ phase showing the pronounced influence on the coordination numbers. The formation of three-dimensional structures, containing several parallel layers of $MoS_2$, may be observed both in unsupported (10, 11) and in supported $MoS_2$ (7, 8). In their rim-edge model, Daage and Chianelli (11) were able to show that the $MoS_2$ edge planes of unsupported multilayered $MoS_2$ slabs also show anisotropy: the top and bottom layers are supposed to contain rim sites active in both hydrodesulfurization (HDS) and hydrogenation (HYD), whereas the layers in between accommodate

[1] Present address: University of Amsterdam, Instituut voor Technische Scheikunde, Nieuwe Achtergracht 166, 1018 WV Amsterdam, The Netherlands. E-mail: hensen@its.chem.uva.nl.

[2] National Centre for HREM, Delft University of Technology, Rotterdamseweg 137, 2628 AL Delft, The Netherlands.

[3] Interfacultair Reactor Instituut, Delft University of Technology, Mekelweg 15, 2629 JB Delft, The Netherlands.



0021-9517/01 $35.00

the edge sites responsible for HDS only. Of particular importance is the study of different support materials because this allows the study of the influence of the Mo–support interaction strength on the catalytic performance (1, 12). The high activity of carbon-supported Mo sulfide catalysts has in part been attributed to the weak metal–carbon interaction (13) and in part to a not-well-understood support effect (3). While silica provides a support with an intermediate metal–support interaction, the use of amorphous silica–alumina (ASA) allows the study of the influence of the support acidity (12).

In the present study, TEM, dynamic oxygen chemisorption (DOC), and EXAFS are used to carefully study the dispersion and stacking degree of the $MoS_2$ phase. With these parameters, the hydrodesulfurization (thiophene and DBT HDS) and hydrogenation (thiophene, DBT, and toluene hydrogenation) activities per mole of Mo are compared for $MoS_2$ on different supports. The aim is to produce a better understanding of the relation between $MoS_2$ morphology and catalytic performance and of the role of the support.

## EXPERIMENTAL

### *Catalyst Preparation*

Important properties of the support materials are listed in Table 1. A series of six catalysts was prepared by pore volume impregnation of the support material (sieve fraction 125–250 $\mu$m, calcination temperature 573 K except for carbon, dried at 383 K) with an amount of an ammonium heptamolybdate (Merck, >97%) solution in ammonia. The final loading of all catalysts as determined by AAS is approximately 7.6 wt% Mo except for Mo–NTA/Al, which has a Mo loading of 6.4 wt%. The NTA-containing catalysts were prepared according to the procedure of Van Veen *et al*. (3). All catalysts were dried for 1 h at room temperature, subsequently at 383 K overnight, and finally (with exception of those prepared with NTA) calcined in static air for 2 h at 723 K after heating to this temperature in 1 h.

To evaluate the acidity effect in the case of the ASA-supported catalyst, the acidic protons of Mo/ASA were exchanged with $Na^+$ analogous to the procedure used for zeolites by Bezman (14). One sample was prepared by impregnating Mo in Na–ASA (Mo/Na–ASA). Na–ASA was obtained by stirring an amount of ASA with a 2.0 M Na–acetate (NaAc) solution for 1 h at room temperature. After filtration, the carrier was washed three times with a 4 mM NaAc solution, before drying in a stove at 383 K overnight. Another sample was prepared by exchanging an amount of sulfided Mo/ASA with NaAc (Mo/ASA–Na) using the same method as described above. The drying step for this last sample was performed at 323 K in a vacuum oven to prevent reoxidation. The amount of Na as determined with AAS was $5 \times 10^{-4}$ mol Na/g for both samples.

**TABLE 1**

**Properties of the Support Materials**

| Support | Designation | Supplier | P.V. (ml/g) | S.A. ($m^2$/g) |
|---|---|---|---|---|
| Carbon | C | Norit RX-3 Extra | 1.0 | 1190 |
| Alumina | Al | Ketjen CK-300 | 0.66 | 263 |
| Silica | Si | Shell | 1.25 | 210 |
| Amorphous Silica–alumina | ASA | Shell | 0.67 | 455 |

### *Transmission Electron Microscopy*

The catalysts were sulfided *quasi in situ* in a mixture of $H_2S/H_2$ (Scott, 10% vol. $H_2S$). The gas flow was kept at 60 ml/min, while the catalyst was heated at a rate of 6 K/min (in the case of Mo–NTA/Al and Mo–NTA/C: 2 K/min) to 673 K. The temperature was then kept at 673 K for 2 h. Subsequently, the sample was cooled to room temperature under flowing He. For details regarding the sample preparation and TEM equipment, the reader is referred to Ref. (15). At least 10 representative micrographs were taken for each catalyst in the high–resolution mode. Typically, the length ($L$) of at least 150 slabs was measured for a catalyst. As a measure for the $MoS_2$ dispersion, the average fraction of Mo atoms at the $MoS_2$ edge surface, denoted as $f_{Mo}$, was calculated assuming that these $MoS_2$ slabs are present as perfect hexagons. For these calculations the data of Kasztelan *et al*. (16) were employed. The $MoS_2$ dispersion ($f_{Mo}$) is statistically evaluated by dividing the total number of Mo atoms at the edge surface by the total number of Mo atoms using the slab sizes determined from the TEM micrographs,

$$f_{Mo} = \sum_{i=1..t} 6n_i - 6 \Big/ \sum_{i=1..t} 3n_i^2 - 3n_i + 1,$$

with $n_i$ being the number of Mo atoms along one side of a $MoS_2$ slab determined from its length ($L = 3.2(2n_i - 1)$ [Å]) (16) and $t$ being the total number of slabs shown by the TEM micrographs. Furthermore, the number of slabs per stack was determined, resulting in an average stacking degree ($N$) calculated by

$$N = \sum_{i=1..t} n_i N_i \Big/ \sum_{i=1..t} n_i,$$

with $n_i$ the number of stacks with $N_i$ layers.

### *Extended X-Ray Absorption Fine Structure*

Catalysts were sulfided according to the procedure described in the previous section and transported in ampules under vacuum. The preparation of the samples was carried

out in an Ar-flushed glove box to prevent oxidation of the sulfided catalysts. Self-supporting wafers giving an absorption $\mu x$ of about 2.5 were pressed using Lonza HSAG-16 expanded graphite. Subsequently, the wafers were placed in an *in situ* EXAFS cell. Measurements were performed on the Swiss–Norwegian beamline at the ESRF in Grenoble (France). Mo K-edge measurements were performed using a gold-coated mirror for harmonics rejection. Si(111) was used as monochromator. The storage ring was operated at 6.0 GeV, while the ring current was in the range of 60–90 mA. Spectra were acquired at liquid $N_2$ temperature. The same data manipulation as described by Sayers and Bunker (17) was employed. The EXAFS results were produced by fitting in *r*-space until a satisfactory fit was obtained for the $k^1$ and $k^3$ weighted FT functions. The fitting procedures were executed with XDAP program version 2.1.5.

### *Dynamic Oxygen Chemisorption*

Dynamic oxygen chemisorption was used to determine the relative dispersion of the different catalysts. For this purpose, 200 mg of catalyst was sulfided *in situ* following the same procedure as for the TEM samples. The catalyst was then cooled to the oxygen chemisorption temperature (333 K) and flushed with He for 1 h. Pulses of 5% vol. $O_2$ in He were injected in the helium carrier gas flow and passed over the catalyst and a thermal conductivity detector. When the effluent peaks had increased to a constant size (less than 1% difference between successive peaks), the total oxygen uptake was calculated.

### *Thiophene Hydrodesulfurization*

Gas-phase thiophene hydrodesulfurization experiments were carried out according to the procedures described in Ref. (18). Overall activities were measured under differential conditions. To estimate first-order rate constants for hydrodesulfurization and hydrogenation, space velocity variation experiments were carried out by varying the total flow between 50 and 150 N ml/min. Both total thiophene conversion and selectivities to desulfurized and hydrothiophene products were determined. As the selectivities for 2,3- and 2,5-dihydrothiophene were much lower than that of tetrahydrothiophene, these partially hydrogenated thiophenes were lumped into the tetrahydrothiophene selectivity.

### *Dibenzothiophene Hydrodesulfurization and Toluene Hydrogenation*

Gas-phase dibenzothiophene (DBT) hydrodesulfurization and toluene hydrogenation experiments were carried out in a stainless steel medium-pressure single-pass microflow reactor. The reactor has an inner diameter of 18 mm and is heated in a three-zone oven. Prior to testing, an amount of catalyst was sulfided *in situ* in a mixture of $H_2S/H_2$ (Scott, 10% vol. $H_2S$) at atmospheric pressure. The gas flow was kept at 200 N ml/min, while the catalyst was heated at a rate of 6 K/min (in the case of Mo–NTA/Al: 2 K/min) to 673 K. The temperature was kept at 673 K for 2 h, before cooling to 573 K in the sulfidation gas mixture. Subsequently, the gas feed was switched to the reactant mixture. This mixture consisted of 200 ppm DBT in hydrogen (DBT HDS) or 1000 ppm toluene in hydrogen (toluene hydrogenation). The hydrogen gas flow was kept at 500 N ml/min by a mass flow controller (Brooks Instruments). The total pressure was then raised to 30 bar. The DBT-containing feed was obtained by dissolving an appropriate amount of DBT (Merck, >98%) in *n*-decane (Merck, >99%), while the toluene-containing feed was obtained by mixing an appropriate amount of toluene (ACROS, >99.5%) with *n*-decane.

The reaction product mixture was analyzed by on-line gas chromatography (Hewlett Packard 5890 series II equipped with a Chrompack CP-SIL 5 CB column). The main products found in DBT HDS were biphenyl (BP), cyclohexylbenzene (CHB), and tetrahydrodibenzothiophene (4H-DBT). No dicyclohexyl was detected under the applied conditions. For toluene hydrogenation, the main product was methylcyclohexane (MCH). In the presence of acid sites (e.g., Mo/ASA), small amounts of ethylcyclopentane, the isomerization product of MCH, and ring-opening products (2-methylhexane, 3-methylhexane) were observed, while $C_4$–, $C_5$–, and $C_6$–products were detected in very small amounts.

## RESULTS AND DISCUSSION

### *TEM, DOC, and EXAFS*

The TEM micrographs clearly show the edge planes of $MoS_2$ slabs oriented in line with or slightly tilted from the electron beam (6). In Figs. 1 and 2, representative TEM micrographs of Mo/Al and Mo–NTA/Al are presented. The $MoS_2$ structures are made up of small ordered sections, which are often bent on a longer scale (see detail in Fig. 1), thus maximizing the interaction with the surface (1). Moreover, some $MoS_2$ structures are observed lying parallel to the support at the edges of the alumina particles, giving substance to the thought that $MoS_2$ indeed lies flat on the support (1, 19). For Mo/Al, the slabs were homogeneously distributed over the surface. On the other hand, Mo–NTA/Al is less homogeneous, the slab lengths are somewhat larger, and the stacking degree also appears to be higher. Mo/Si is rather inhomogeneous, i.e., in addition to areas containing multi-layered long slabs and nestlike structures; also areas with a very low slab density are present. Figure 3 shows a representative TEM micrograph of sulfided Mo/ASA. This sample is also rather inhomogeneous and shows quite some stacking. Also, nestlike structures consisting of up to seven slabs per stack can be found (inset to Fig. 3). TEM/EDX

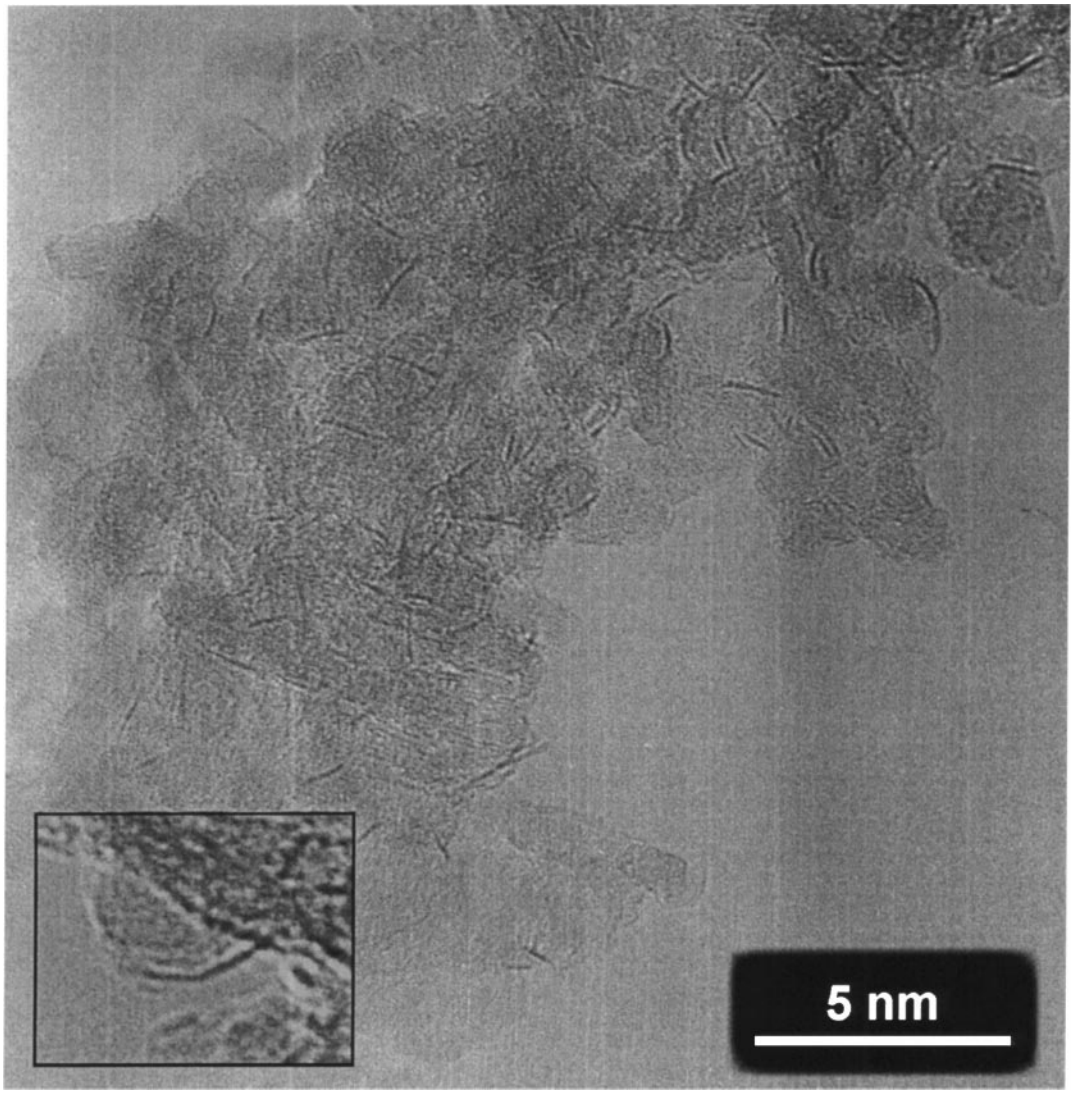


**FIG. 1.** TEM image of sulfided Mo/Al. The inset shows a magnification (6×) of a bent $MoS_2$ along an alumina particle.

data of a sample similar to Mo/ASA, i.e., sulfided 8 wt% Mo/ASA (Si/Al = 80/20 w/w, consisting of 60 wt% ASA and 40 wt% alumina), show that the loading on the ASA part was 2.1 wt% Mo and on the alumina part 18 wt%. This preference for alumina is in line with the results of an Mo equilibrium adsorption study comparing alumina and ASA supports (20).

In addition to the $MoS_2$ phase, nanometer-sized entities were observed in the present set of catalysts. These entities are thought to be partially sulfided Mo-containing species similar to the ones observed for tungsten-based catalysts (21). In the tungsten case, the contribution of such species to the catalytic activity is significant. From an analysis of our TEM micrographs, it is deduced that the number of these entities is low for Mo-based catalysts. This relates to the ease of sulfidation of Mo compared to that of W (22). The composition of these species is the subject of a separate study (23). The TEM micrographs of Mo/C show strange fringelike patterns with a very irregular structure. By comparison with the sulfided native carbon support, it was found that this is an intrinsic phenomenon of the carbon support. Therefore, it appeared impossible to accurately determine $MoS_2$ slab lengths from these TEM micrographs. The $MoS_2$ slabs that were found at positions where they extend into the vacuum with no other carbon material between the electron beam and the detection section exhibited the same *d*-spacing (3.03 Å)as the slabs in Mo/Al.

In an effort to quantify the differences in $MoS_2$ dispersion, the slab length and number of slabs per stack were determined for the sulfided catalysts (except for Mo/C). The slab length distributions for Mo/Al and Mo–NTA/Al are shown in Fig. 4. Mo/Al clearly shows smaller slabs than Mo–NTA/Al, and its slab length distribution is also narrower. As

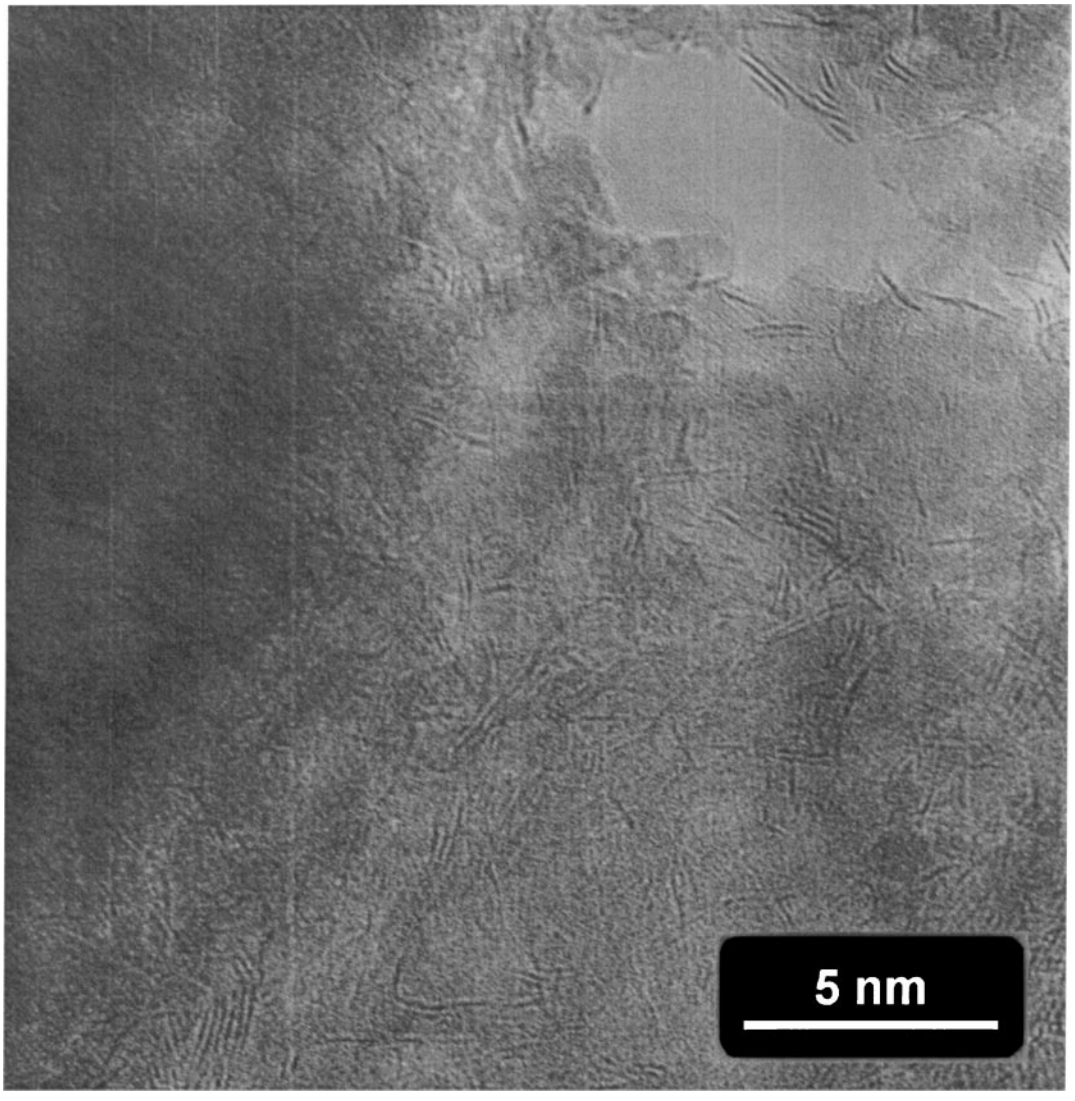


**FIG. 2.** TEM image of sulfided Mo–NTA/Al.

a measure for the dispersion, average slab lengths are often calculated from these distributions (8, 24). A more detailed comparison can be made by calculating the total amount of Mo atoms available for reaction as outlined above. It is well accepted that most hydrotreating reactions take place at the $MoS_2$ edge surface (1, 25). An inherent approximation in this calculation (and in those in the mentioned literature, for that matter) is that the catalytic activity is regarded uniform at the $MoS_2$ edge surface, which is an approximation in view of the difference in activity for corner and edge sites (25). Both $f_{Mo}$ and the average stacking degree ($N$) for the various catalysts are listed in Table 2. To demonstrate that the use of the average slab length can lead to erroneous results, this parameter for Mo/Al ($L = 19.8$ Å)and Mo/ASA ($L = 28.9$ Å)is converted into a value for the $MoS_2$ edge dispersion as if there was a uniform slab length for the given catalysts. This yields the values $f_{Mo} = 0.54$ and $f_{Mo} = 0.39$ for Mo/Al and Mo/ASA, respectively. The value for Mo/ASA is different from the one determined by our method.

Comparing Mo/Al and its NTA-promoted counterpart reveals that the use of NTA indeed reduces the interaction between Mo and the support (3), leading to a more

**TABLE 2**

**Fraction Available Mo ($f_{Mo}$) and Average Stacking Degree ($N$)**

| Catalyst | $f_{Mo}$ | $N$ |
|---|---|---|
| Mo/Al | 0.49 | 1.4 |
| Mo–NTA/Al | 0.34 | 1.7 |
| Mo/Si | 0.23 | 2.7 |
| Mo/ASA | 0.30 | 2.5 |

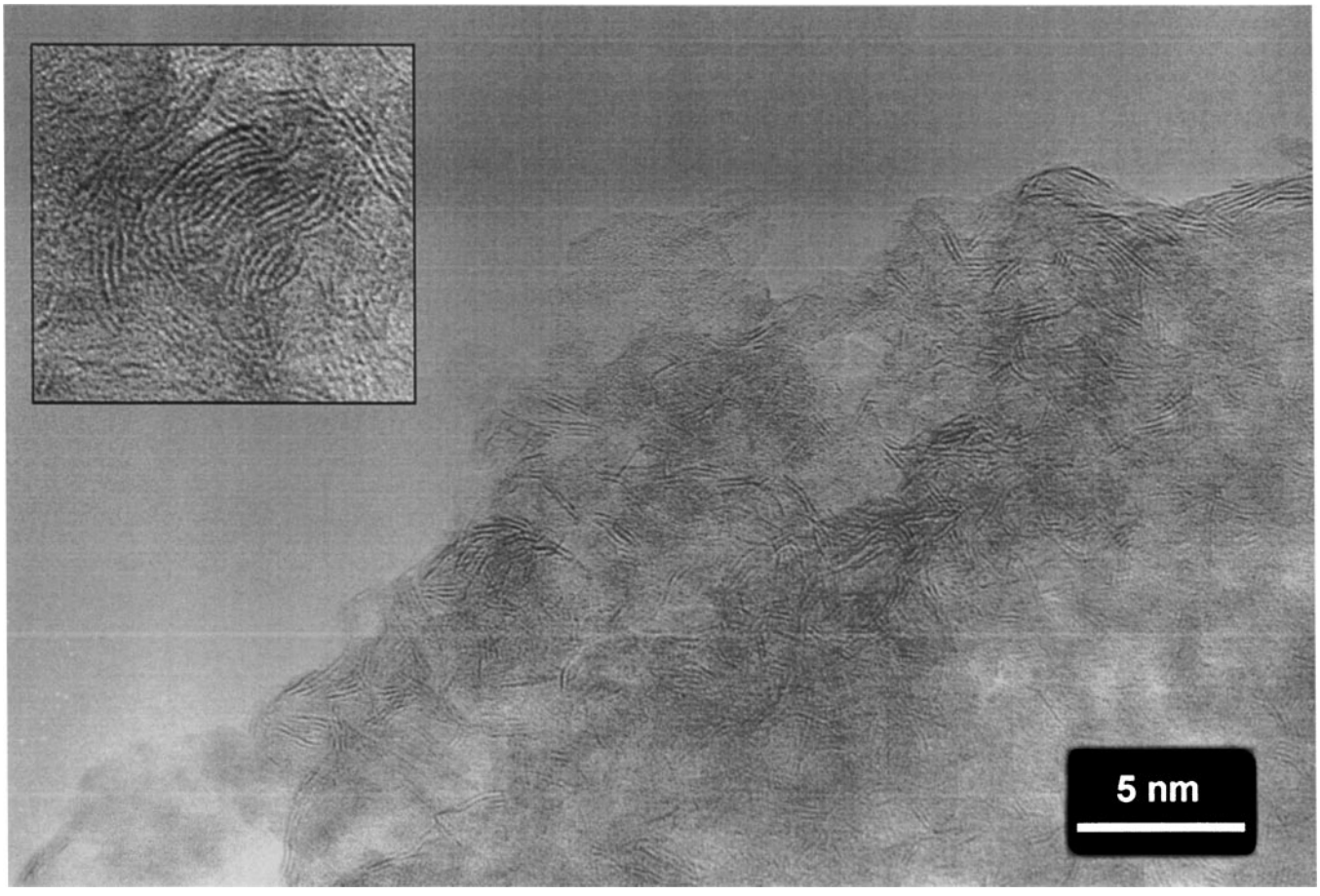


**FIG. 3.** TEM image of Mo/ASA. The inset shows a magnification (4×) of a nest consisting of several multilayered $MoS_2$ stacks.

stacked $MoS_2$ phase. The strong metal–support interaction in Mo/Al hinders sintering of the $MoS_2$ slabs (1, 19), resulting in a dispersed $MoS_2$ phase. The stacking degree in Mo/Si is much higher than that in the alumina-supported samples. This is due to the lower metal–support interaction for the silica support, which leads to a type II $MoS_2$ phase (4, 19). The long slab lengths of sulfided Mo/Si result from the low dispersion in the oxide precursor (26). Whereas the alumina-supported catalysts show mostly single-layered slabs and small numbers of three-dimensional structures having two

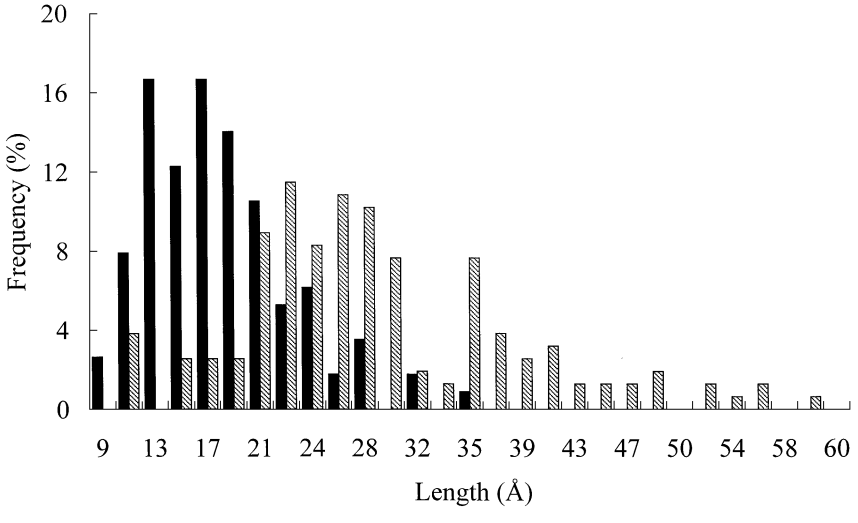


**FIG. 4.** Slab length distribution (black, Mo/Al; gray, Mo-NTA/Al; length axis indicates average of length interval, e.g., 13 Å means 12–14 Å).

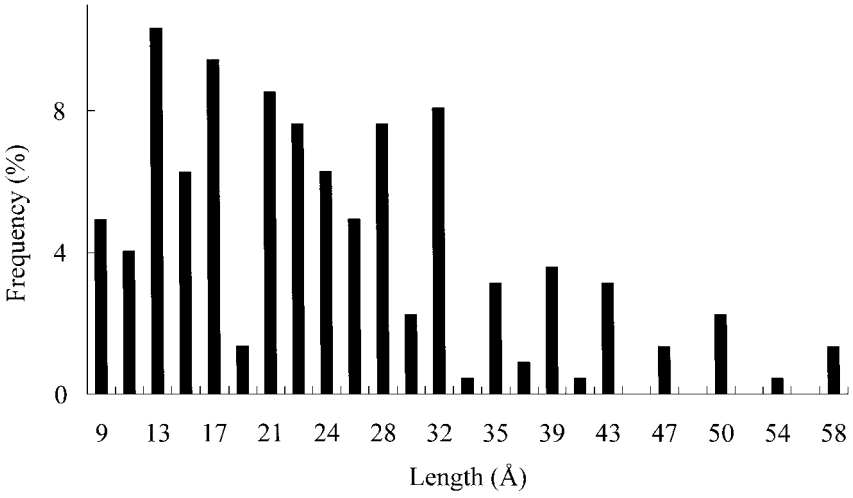


**FIG. 5.** Slab length distribution for sulfided Mo/ASA.

or three layers, Mo/Si and Mo/ASA mostly show multilayered slabs with up to seven $MoS_2$ layers. The dispersion of Mo/ASA is in between that of the alumina- and silica-supported catalysts. From the slab length distribution depicted in Fig. 5, it can be seen that this catalyst exhibits a broad slab length distribution. This support consists of small alumina islands in an amorphous silica-alumina matrix. Since $MoS_2$ is preferentially situated on this alumina part, it forms small stacked slabs.

The present results agree well with data obtained by Mauchausse *et al.* (24), who also observed a higher average slab length and a higher stacking degree for silica-supported $MoS_2$ than for alumina-supported $MoS_2$. Payen *et al.* (8) concluded that for a set of alumina-supported Mo sulfide catalysts with different metal loading the stacking degree is between 1.4 and 2.7 layers, depending on the use of promoters and additives. This is in excellent agreement with the present results. However, the average slab length for Mo/Al in the present study ($L = 19.8$ Å) is shorter than the one observed by Payen and co-workers (8) for a comparable catalyst ($L = 32$ Å). Relevant experimental differences with the present study are a lower sulfidation temperature (623 K), air exposure during the preparation of the TEM samples, and a lower magnification in their study. Whilst still subject to the same differences, Da Silva *et al.* (27) determined an average slab length of 25 Å with an average stacking degree of 1.2 for a catalyst similar to the present Mo/Al.

To obtain a measure of the $MoS_2$ dispersion for Mo/C, the oxygen uptake for this catalyst was compared to that of the catalysts with known $f_{Mo}$. The total oxygen uptake, the oxygen uptake per mole of Mo as well as the intrinsic oxygen uptake are listed in Table 3. The intrinsic oxygen uptake is calculated by correcting the oxygen uptake per mole of Mo for the differences in dispersion. It appears that this intrinsic oxygen uptake is nearly constant for the catalysts. This is strong indication that we have observed a representative fraction of the total $MoS_2$ present to calculate $f_{Mo}$. Although very small $MoS_2$ particles may be present, it appears that their number is relatively small and does not influence the dispersion parameter to a large extent. To validate this, a quantitative assessment similar to the one by Eijsbouts *et al.* (7) is necessary. The intrinsic oxygen uptake for these catalysts was averaged (0.30 mol/mol of $Mo_{available}$) and assumed to be a constant. A value of $f_{Mo} = 0.73$ is calculated for Mo/C. No information on the stacking degree for this catalyst is available. On the one hand, $N$ is expected to be low due to the very high surface area of the activated carbon support, although a significant part of the pore volume may not be accessible due to the microporous structure of this type of carbon. On the other hand, the low metal–support interaction may lead to the formation of three-dimensional $MoS_2$ structures. Such large structures that would be clearly seen with TEM seem to be absent.

Since there remains a large gap between slab sizes determined from our TEM analyses and EXAFS results in the literature (4, 5), Mo K-edge EXAFS were performed on the

**TABLE 3**

**Oxygen Uptake of the Different Catalysts**

| Catalyst | Uptake ($\mu$mol/g) | Uptake (mol of O/mol of Mo) | Intrinsic uptake (mol of O/mol of $Mo_{avail.}$) |
|---|---|---|---|
| Mo/C | 176 | 0.22 | — |
| Mo/Al | 115 | 0.15 | 0.31 |
| Mo–NTA/Al | 75 | 0.098 | 0.29 |
| Mo/Si | 54 | 0.072 | 0.31 |
| Mo/ASA | 65 | 0.094 | 0.30 |

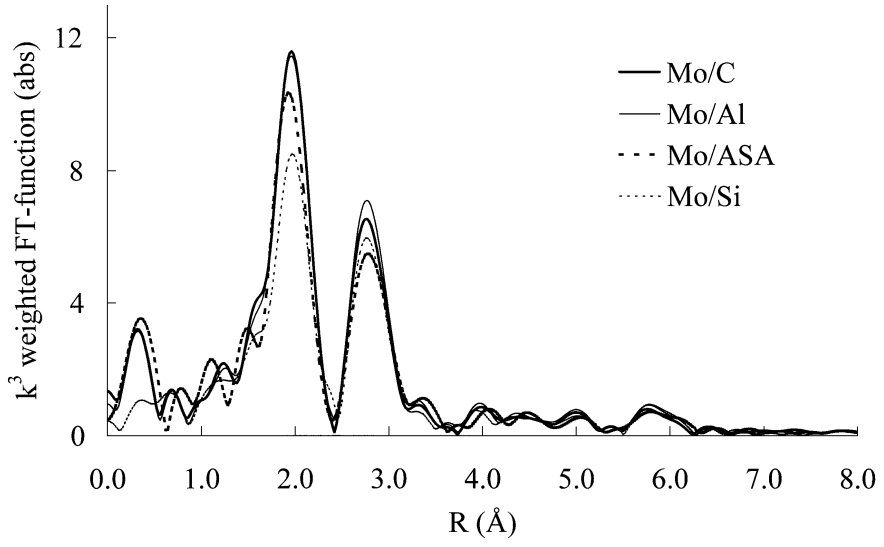


**FIG. 6.** Radial distribution function for Mo K-edge EXAFS in sulfided Mo/C, Mo/Al, Mo/Si, and Mo/ASA.

sulfided catalysts. Classical calculations of $MoS_2$ dispersion from EXAFS data (1, 4, 5) underestimate the $MoS_2$ slab size due to structural disorder. Shido and Prins (9) showed that the introduction of some disorder in the position of Mo atoms in a $MoS_2$ slab (depending on the position of the Mo atom within the slab) can explain the low Mo–Mo coordination numbers. The EXAFS radial distribution functions of sulfided Mo/C, Mo/Al, Mo/Si, and Mo/ASA are presented in Fig. 6. These data could be well analyzed using one Mo–S coordination at a distance of 2.38 Å and one Mo–Mo coordination at 3.12 Å. This clearly indicates the presence of $MoS_2$ crystallites (4, 5). The numerical Mo EXAFS results are presented in Table 4.

The data for Mo/C are in good agreement with those obtained by Bouwens *et al.* (5), while the present results for Mo/Al show a somewhat lower Mo–Mo coordination than the one determined by Bouwens *et al.* (28) to be attributed to the higher calcination temperature (823 K) applied by these authors. While the Mo–Mo coordination number for Mo/ASA is only somewhat lower than that for Mo/Al and Mo/C, this coordination number is considerably reduced for Mo/Si. At first sight, this would suggest that the $MoS_2$ slab size in the catalysts supported by the refractory oxides is smaller than that for the carbon-supported one. The application of the model put forward by Shido and Prins (9) should in principle allow us to correlate the Mo–Mo coordination numbers from the EXAFS analysis to the slab lengths determined from the statistical TEM analysis. The overall trend in coordination number is opposite to the one obtained by TEM. Hence, such an evalution will not lead to a better match. Besides the effect of dispersion on the coordination number, the local ordering of the $MoS_2$ phase may also vary. Walton and Hibble (29) showed that the W–W and W–S coordination numbers of $WS_2$ prepared by thermal decomposition of the tetrathiotungstate are significantly reduced from those in crystalline $WS_2$. This was attributed to the intermediate formation of a highly amorphous $WS_3$ phase during decomposition of the thiosalt. In a similar fashion, the crystallinity of the supported $MoS_2$ particles might be dependent on the sulfidation mechanism. Amongst others, this will depend on the structure of the oxide precursor and the degree of support interaction. For instance, due to the very weak Mo-activated carbon interaction, Mo/C sulfidation is essentially completed at 560 K (13). The higher final sulfidation temperature will result in a well-crystallized $MoS_2$ phase. Mo/Si is known to form bulky $MoO_3$ structures upon calcination (26). Sulfidation of these structures may be more difficult, leading to a $MoS_3$–$MoS_2$ transformation at higher temperatures than those in Mo/C. The resulting $MoS_2$ phase may be less crystalline. The interpretation of the EXAFS results is not conclusive, although the important point to be made is that the local disorder

**TABLE 4**

**Mo K-Edge EXAFS Fit Parameters of Selected Catalysts**

| Catalyst | Backscatter | $N$ | $R$ (Å) | $\Delta\sigma^2$ ($10^{-3}$Å$^2$) | $\Delta E_0$ (eV) |
|---|---|---|---|---|---|
| Mo/C | Mo–S | 5.1 | 2.39 | 1.5 | 2.4 |
| | Mo–Mo | 2.8 | 3.11 | 2.6 | 2.1 |
| Mo/Al | Mo–S | 4.9 | 2.38 | 1.2 | 2.7 |
| | Mo–Mo | 2.6 | 3.12 | 1.7 | 1.4 |
| Mo/Si | Mo–S | 3.8 | 2.38 | 0.5 | 3.1 |
| | Mo–Mo | 2.0 | 3.13 | 1.7 | 0.1 |
| Mo/ASA | Mo–S | 4.6 | 2.38 | 1.4 | 2.0 |
| | Mo–Mo | 2.5 | 3.12 | 2.2 | 0.6 |

*Note.* Estimated accuracies: $N \pm 20\%$, $R \pm 0.04$ Å, $\Delta\sigma^2 \pm 20\%$, $\Delta E_0 \pm 10\%$. $MoS_2$: $N_{Mo-S} = 6$, $R_{Mo-S} = 2.41$ Å; $N_{Mo-Mo} = 6$, $R_{Mo-Mo} = 3.16$ Å.

**TABLE 5**

**Kinetic Parameters for Thiophene HDS (623 K, 1 bar, Activities in mol (mol h); Intrinsic Rate Constants in $10^3$/(Pa h)**

| | Mo/C | Mo/Al | Mo–NTA/Al | Mo/Si | Mo/ASA |
|---|---|---|---|---|---|
| Overall HDS activity | 3.69 | 0.95 | 1.2 | 0.9 | 1.3 |
| Intrinsic HDS activity | 4.9 | 2.0 | 3.5 | 3.9 | 4.3 |
| $k_{HDS}$ | 1.43 | 0.75 | 1.15 | 0.70 | 0.10 |
| $k_{HYD}$ | 0.25 | 0.023 | 0.070 | 0.11 | 0.32 |
| $k_{HYD}/k_{HDS}$ | 0.17 | 0.031 | 0.061 | 0.16 | 3.2 |

between the various catalysts strongly varies. This affects the coordination numbers in addition to the effect of particle size.

*Thiophene HDS*

The standard thiophene HDS reaction rates (differential conditions, 623 K, $6 \times 10^3$ Pa thiophene, $1 \times 10^3$ Pa $H_2S$) for our set of catalysts are listed in Table 5. These reaction rates are expressed both on a per mole of total Mo present (overall HDS activity) as well as on a per mole of available Mo (intrinsic HDS activity) basis. This last activity parameter is obtained by correcting for differences in Mo dispersion by using $f_{Mo}$ and represents the turnover frequency.

Whereas the overall HDS activity of Mo–NTA/Al is only slighter higher than that of Mo/Al, the intrinsic activity of Mo–NTA/Al is markedly higher than that of Mo/Al, the difference being almost equal to the one observed for their Co-promoted counterparts (3). Mo/Si exhibits the lowest overall activity to be explained by the poor $MoS_2$ dispersion. The intrinsic activity, however, is higher than that of the alumina-supported catalysts. Two important conclusions can be drawn. First, the large differences in $MoS_2$ dispersion determine the activity ranking to a large extent. Secondly, a higher stacking degree appears to be beneficial for the thiophene HDS activity. The strong metal–support interaction for Mo/Al yields a dispersed $MoS_2$ phase with low stacking degree. The higher stacking degree in Mo–NTA/Al permits a higher thiophene HDS activity, albeit that the dispersion is significantly reduced. The higher intrinsic thiophene HDS activity for Mo/Si thus relates to the higher stacking degree. The activity of Mo/ASA is close to that of Mo/Si, having a similar stacking degree.

To evaluate the effect of the acidity of the ASA-supported catalyst, the two samples treated with NaAc (Mo/Na–ASA and Mo/ASA–Na) were tested in a standard thiophene HDS experiment. Both Mo/Na–ASA and Mo/ASA–Na showed slightly lower overall HDS activities (1.2 mol/mol h) than the untreated one, indicating that the presence of acid sites has a small positive effect. The intrinsic activity of Mo/ASA–Na is equal to the one found for Mo/Si. This result suggests that the major factor in high intrinsic HDS activity is the high stacking degree.

To determine thiophene hydrodesulfurization and hydrogenation reaction rate constants, results of space velocity variation experiments were fitted, assuming first-order kinetics for the HDS of thiophene and tetrahydrothiophene and for the hydrogenation of thiophene to THT, similar to the reaction network proposed by Leglise *et al.* (30). The rate constants were fitted using a third-order Runga–Kutta method. For example, the mole fractions versus space velocity are given for Mo/C in Fig. 7 together with the fitted mole fractions. It was found that the first-order HDS rate constant for tetrahydrothiophene is approximately ten times higher than the one for thiophene. The kinetic parameters for the different catalysts are listed in Table 5.

The highest overall activity for Mo/C stems from both a high intrinsic thiophene HDS rate constant ($k_{HDS}$) and a high intrinsic thiophene hydrogenation rate constant ($k_{HYD}$). The HDS rate constant for Mo/Al is about half that of Mo/C, while $k_{HYD}$ is lowered by about an order of magnitude. The desulfurization route via THT appears to be of greater importance for Mo/C. More complete sulfidation in Mo–NTA/Al leads to increases in both $k_{HDS}$ and $k_{HYD}$. However, the hydrogenation/hydrodesulfurization ratio ($k_{HYD}/k_{HDS}$) is larger for this catalyst than for Mo/Al. This ratio is even higher for Mo/Si and exceptionally high for Mo/ASA. For the latter catalyst, the desulfurization via THT is clearly important. The hydrogenation rate constant of Mo/ASA is even higher than the one calculated for Mo/C.

The use of carbon results in high HDS and hydrogenation rate constants to be attributed to the absence of strong metal–support interaction. Moreover, in view of the very high dispersion for Mo/C, one expects that the ratio of corner to edge sites is exceptionally high for this catalyst. The sulfur atoms associated with these corner Mo atoms are terminal ones (16, 31) and it has been argued that these corner

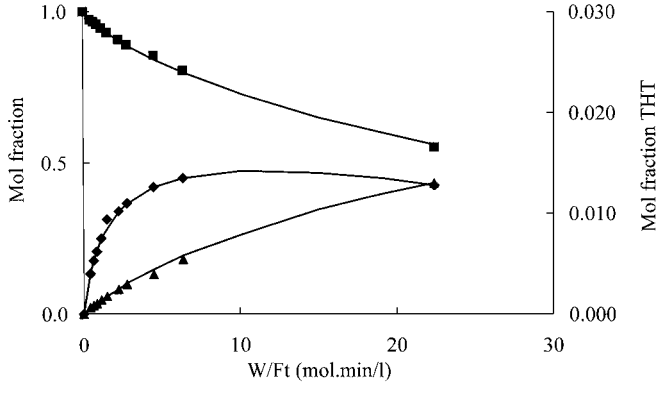


**FIG. 7.** Mole fractions during thiophene HDS (atmospheric pressure, 623 K) for Mo/C as a function of space velocity: (■) thiophene; (▲) $C_4$ products; (◆) THT (right axis); the solid lines represent the fit obtained after modelling.

atoms have a higher degree of coordinative unsaturation than the edge sites (31). This facilitates $\pi$-complexation required for aromatic-ring hydrogenation (1). Hence, it is expected that the high hydrogenation rate constant for Mo/C relates to the large number of corner sites. Based on the value of $f_{Mo} = 0.73$ for Mo/C, the corner site fraction is calculated to be 0.56. Notably, this fraction is much smaller for the other catalysts and ranges from 0.29 for Mo/Al to 0.18 for Mo/Si. This results in a strong decrease of the hydrogenation rate constant when $MoS_2$ is supported on the refractory oxides, while $k_{HDS}$ is reduced to a lesser extent. Only Mo/ASA shows an exceptionally high $k_{HYD}$.

Interestingly, the ratio $k_{HYD}/k_{HDS}$ increases with increasing stacking degree, comparing Mo/Al, Mo–NTA/Al, and Mo/Si. While the number of corner sites decreases, it appears that the increase in the stacking degree is beneficial for thiophene hydrogenation. These results are to be compared to the one obtained by Daage and Chianelli (11). These authors found that the hydrogenation/hydrodesulfurization ratio obtained from liquid-phase DBT HDS decreased when the stacking degree of unsupported $MoS_2$ particles increased. However, a relevant comparison with the present data is difficult to make since the stacking degree of these $MoS_2$ particles was varied between 3 and 1000. The number of slabs per stack for the supported $MoS_2$ is not uniform and the average stacking degree remains below 3. Hence, the activity of these $MoS_2$ particles cannot be discussed in terms of rim and edge sites as proposed by Daage and Chianelli (11). Moreover, one has to be extremely careful comparing activities obtained under very different reaction conditions, i.e., in the gas and liquid phase. It has been shown that there exists a remarkable difference in ranking when HDS activities are compared from experiments carried out in the gas or liquid phase (32). In that communication, it is proposed that the formation of a condensed liquid plays a decisive role in the activity ranking of HDS catalysts.

In line with the rim-edge model, it appears that the selectivities are influenced by the specific morphology of the $MoS_2$ layers. However, we propose that easier $\pi$-complexation with molecules containing aromatic rings results from an increased accessibility of the $MoS_2$ layers not directly attached to the support. The "planar" adsorption of thiophene is suggested to precede hydrogenation of the aromatic ring, while a "perpendicular" one-point adsorption through the S atom leads to desulfurization (1, 33). The results obtained for Mo/ASA indicate that the high overall HDS activity for this catalyst must be attributed to a very high $k_{HYD}$, resulting in a preferred desulfurization route via THT. Since the morphology of this catalyst resembles the one of Mo/Si and reducing the acidity does not markedly influence the overall activity, it is tentatively concluded that the support induces this peculiar behavior. Whether this is an effect of electronic nature remains elusive. However, another important factor can also be the lower crystallinity of the alumina islands of the ASA support on top of which the $MoS_2$ species are preferentially located in this system.

The present data show that the selectivities are profoundly dependent on the morphology of the $MoS_2$ phase and type of support. The different morphologies are a consequence of the type of support, most importantly, the extent of metal–support interaction. Moreover, the support also appears to directly influence the individual reaction rates. The higher intrinsic rates for the carbon-supported catalyst and the extremely high hydrogenation rate constant for Mo/ASA show this. This latter effect is most probably of an electronic nature but the fundamental basis to its understanding is still lacking.

### *Dibenzothiophene HDS*

The conversion of DBT as a function of the space velocity for Mo/C is presented in Fig. 8. Since there was some DBT conversion in the blank experiment, this measurement was included. The yield of 4H-DBT goes through a maximum, showing that this is an intermediate product in the HDS of DBT in agreement with results by Daage and Chianelli (11). These data were modelled by assuming pseudo-zero-order kinetics according to the reaction scheme from Ref. (11). DBT is either directly desulfurized to BP or hydrogenated to 4H-DBT, which yields CHB after sulfur extrusion. A separate experiment with a feed containing BP besides DBT showed that there was no direct conversion of BP into CHB. Although BP hydrogenation readily proceeds over sulfide catalysts (34), the absence of BP hydrogenation under the applied conditions is explained by the much higher heat of adsorption of DBT. The rate constants were fitted using a third-order Runga–Kutta method. The kinetic parameters for the different catalysts can be found in Table 6.

It was found that the HDS rate constant for 4H-DBT was approximately 13 times higher than the one for DBT.

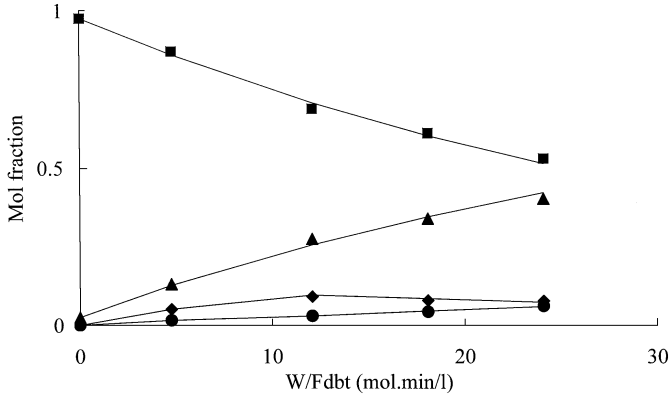


**FIG. 8.** Mole fractions during DBT HDS (30 bar, 573 K) for Mo/C as a function of space velocity: (■) DBT; (▲) BP; (◆) 4H-DBT; (●) CHB; the solid lines represent the fit obtained after modelling.

**TABLE 6**

**Intrinsic Kinetic Parameters for DBT HDS (573 K, 30 bar, 200 ppm DBT, All Parameters in mol (mol /h)**

| | Mo/C | Mo/Al | Mo–NTA/Al | Mo/Si | Mo/ASA |
|---|---|---|---|---|---|
| $k_{HDS}$ | 33 | 31 | 51 | 96 | 53 |
| $k_{HYD}$ | 5.5 | 6.5 | 11 | 17 | 33 |
| $k_{HYD}/k_{HDS}$ | 0.17 | 0.21 | 0.22 | 0.18 | 0.62 |

On the basis of the intrinsic rate constants for desulfurization ($k_{HDS}$, the rate constant for direct DBT HDS) and hydrogenation ($k_{HYD}$, the rate constant for DBT hydrogenation to 4H-DBT), it is found that the trends agree with the trends found for the intrinsic thiophene HDS and hydrogenation rate constants. Both $k_{HDS}$ and $k_{HYD}$ increase, going from Mo/Al via Mo-NTA/Al to Mo/Si, while Mo/ASA shows an intermediate HDS, but the highest hydrogenation rate constant. Surprisingly, Mo/C now exhibits small intrinsic rate constants similar to Mo/Al. Moreover, the ratio $k_{HYD}/k_{HDS}$ is relatively constant with the exception of that for Mo/ASA. It now appears that a higher stacking degree improves both the intrinsic DBT HDS and hydrogenation activity to the same extent. Whereas it was proposed that a planar coordination of thiophene is important for hydrogenation and a perpendicular one is the precursor for desulfurization, the DBT HDS results may indicate that HDS and hydrogenation of DBT occur via a common planar-oriented adsorption mode. Such an adsorption mode is in line with the observation of the higher intrinsic $k_{HDS}$ and $k_{HYD}$ with increasing stacking degree. From organometallic studies, it is indeed known that the usual adsorption mode of DBT is $\eta^6$ through the benzene ring (1, 35, 36), although there is also proof for $\eta^1$-S coordination (35). The low intrinsic activities observed for Mo/C in DBT HDS can be tentatively explained by steric hindrance of the support in a planar adsorption mode of the large DBT molecule, provided that the stacking degree is low for Mo/C.

*Toluene Hydrogenation*

The intrinsic toluene hydrogenation first-order reaction rate constants are collected in Table 7. These results show that Mo/Si has the highest activity followed by Mo–NTA/Al and Mo/Al. The intrinsic hydrogenation activity for Mo/ASA is even higher than that for Mo/C. These results are in good agreement with the trends in intrinsic thiophene hydrogenation rate constants. This may not be very surprising since the routes for hydrogenation of thiophene and toluene may require similar adsorption modes. As mentioned before, this involves a planar $\pi$-complex as a precursor for the hydrogenation of small molecules with an aromatic ring. Similar to the case of thiophene hydrogenation, the intrinsic hydrogenation rate for toluene increases with increasing stacking degree. The high hydrogenation activity for Mo/C stresses the importance of the corner sites as sites responsible for hydrogenation. The very high hydrogenation activity of Mo/ASA seems to be a general phenomenon since this was also found for thiophene and DBT hydrogenation. Moreover, recent results by Robinson *et al.* (37) indicate that the high activity of promoted ASA-supported $MoS_2$ in the hydrodesulfurization of (substituted) DBT is to be attributed to high hydrogenation activity.

**TABLE 7**

**Reaction Rate Constants for Toluene Hydrogenation (573 K, 30 bar, 1000 ppm Toluene, All Parameters in mol/(mol h)**

| | Reaction rate constant |
|---|---|
| Mo/C | 7.3 |
| Mo/Al | 2.9 |
| Mo–NTA/Al | 3.4 |
| Mo/Si | 5.2 |
| Mo/ASA | 8.7 |

## CONCLUSIONS

The present results show that the use of different support materials for $MoS_2$ induces large differences in dispersion and morphology. These morphological changes were evaluated by a statistical TEM analysis, yielding two important parameters, i.e., the fraction of Mo atoms located at the edge surface of the $MoS_2$ slabs and the average stacking degree. The EXAFS analysis shows that the local ordering in $MoS_2$ between the catalysts varies strongly, implying that the present comparisons relating intrinsic activity to $MoS_2$ morphology are only a first approximation. While the use of NTA leads to a higher stacking degree for alumina-supported $MoS_2$, the $MoS_2$ dispersion of such a catalyst is considerably lower. This is explained by a decreased metal–support interaction. Sulfidation of silica-supported Mo results in a poorly dispersed $MoS_2$ phase with a high degree of stacking. The use of amorphous silica–alumina enables one to prepare a $MoS_2$ phase with a stacking degree similar to the silica-supported one, but with an improved $MoS_2$ dispersion. A comparison of the oxygen chemisorption capacity of this catalyst with those supported by the refractory oxides shows that the dispersion of the carbon-supported $MoS_2$ phase is the highest.

The intrinsic hydrogenation rate constant for small molecules such as thiophene and toluene increases with an increasing degree of stacking, showing that a planar adsorption mode through the aromatic ring is the one required for hydrogenation. While the intrinsic thiophene HDS rate constant is not a strong function of the stacking degree, this DBT HDS rate constant increases with the stacking degree. This is explained by a perpendicular adsorption mode through the S atom for thiophene and a planar one for the

larger DBT molecule. Due to the high $MoS_2$ dispersion on the carbon support, the number of corner sites is exceptionally high, leading to high hydrogenation activities. This last parameter is strongly reduced for the oxide-supported catalysts. The intrinsic activity in DBT HDS for Mo/C is comparable to that of alumina-supported $MoS_2$, which results from a hampered planar adsorption of DBT. Supporting $MoS_2$ on ASA yields an interesting system with exceptionally high hydrogenation activity, although the nature of this support effect is not fully understood.

It appears that the morphology of the active $MoS_2$ phase and the choice of support have a profound influence on the intrinsic gas-phase hydrodesulfurization and hydrogenation selectivities. Such relationships also depend on the size of the reactant molecule.

## ACKNOWLEDGMENTS

These investigations were supported by the Netherlands Foundation for Chemical Research (SON) with financial aid from the Netherlands Technology Foundation (STW). The research was performed under the auspices of NIOK, the Netherlands Institute for Catalysis Research, Lab Report TUE-2000-5-4.

## REFERENCES

1. Topsøe, H., Clausen, B. S., and Massoth, F. E., "Hydrotreating Catalysis." Springer, Berlin, 1996.
2. Candia, R., Sorensen, O., Villadsen, J., Topsøe, N.-Y., Clausen, B. S., and Topsøe, H., *Bull. Soc. Chim. Belg.* **93**, 763 (1984).
3. Van Veen, J. A. R., Gerkema, E., Van der Kraan, A. M., and Knoester, A., *J. Chem. Soc. Chem. Commun.* 1684 (1987).
4. Clausen, B. S., Topsøe, H., Candia, R., Villadsen, J., Lengeler, B., Als-Nielsen, J., and Christensen, F., *J. Phys. Chem.* **85**, 3868 (1982).
5. Bouwens, S. M. A. M., Van Veen, J. A. R., Koningsberger, D. C., De Beer, V. H. J., and Prins, R., *J. Phys. Chem.* **95**, 123 (1991).
6. Delannay, F., *Appl. Catal.* **16**, 135 (1985).
7. Eijsbouts, S., Heinerman, J. J. L., and Elzerman, H. J. W., *Appl. Catal. A* **105**, 53 (1993).
8. Payen, E., Hubaut, R, Kasztelan, S., Poulet, O., and Grimblot, J., *J. Catal.* **147**, 123 (1994).
9. Shido, T., and Prins, R., *J. Phys. Chem. B* **102**, 8426 (1998).
10. Klier, K., *Catal. Today* **15**, 361 (1992).
11. Daage, M., and Chianelli, R. R., *J. Catal.* **149**, 414 (1994).
12. Luck, F., *Bull. Soc. Chim. Belg.* **100**, 11–12 (1991).
13. Vissers, J. P. R., Scheffer, B., De Beer, V. H. J., Moulijn, J. A., and Prins, R., *J. Catal.* **105**, 277 (1987).
14. Bezman, R., *Catal. Today* **13**, 143 (1992).
15. Kooyman, P. J., Zandbergen, H. W., and Van Langeveld, A. D., *in* "Conference Proceedings vol. 2, ICEM 14 (International Conference on Electron Microscopy), Mexico, 1998," pp. 491–492.
16. Kasztelan, S., Toulhoat, H., Grimblot, J., and Bonnelle, J. P., *Appl. Catal.* **13**, 127 (1984).
17. Sayers, D. E., and Bunker, B. A., *in* "X-Ray Absorption: Principles, Applications, Techniques of EXAFS, SEXAFS and XANES" (Koningsberger, D. C., and Prins, R., Eds.), p. 211. Wiley, New York, 1988.
18. Hensen, E. J. M., Brans, H. J. A., Lardinois, G. M. H. J., De Beer, V. H. J., Van Veen, J. A. R., and Van Santen, R. A., *J. Catal.* **192**, 98 (2000).
19. Srinivasan, S., Datye, A. K., and Peden, C. H. F., *J. Catal.* **137**, 413 (1992).
20. Vissenberg, M. J., Heffels, M. M. E. H, Joosten, L. J. M., Van Welsenes, A. J., De Beer, V. H. J., Van Santen, R. A., and Van Veen, J. A. R., submitted.
21. Reinhoudt, H. R., Van Langeveld, A. D., Kooyman, P. J., Stockmann, R. M., Prins, R., Zandbergen, H. W., and Moulijn, J. A., *J. Catal.* **179**, 443 (1998).
22. Mangnus, P. J., Scheffer, B., and Moulijn, J. A., *Am. Chem. Soc., Pet. Div. Prepr.* **32**, 329 (1987).
23. Kooyman, P. J., Hensen, E. J. M., De Jong, A., Niemantsverdriet, J. W., and Van Veen, J. A. R., submitted.
24. Mauchausse, C., Mozzanega, H., Turlier, P., and Dalmon, J. A., "Proceedings, 9th International Congress on Catalysis, Calgary, 1988" (M. J. Philips and M. Ternan, Eds.), p. 775. Chem. Institute of Canada, Ottawa, 1988.
25. Eijsbouts, S., *Appl. Catal. A* **158**, 53 (1997).
26. Del Arco, M., Carrazán, S. R. G., Martín, C., Martín, I., Rives, V., and Malet, P., *J. Mater. Chem.* **3**, 1313 (1993).
27. Da Silva, P., Marchal, N., and Kasztelan, S., *Stud. Surf. Sci. Catal.* **106**, 353 (1997).
28. Bouwens, S. M. A. M., Van Zon, F. B. M., Van Dijk, M. P., Van der Kraan, A. M., De Beer, V. H. J., Van Veen, J. A. R., and Koningsberger, D. C., *J. Catal.* **146**, 375 (1994).
29. Walton, R. I., and Hibble, S. J., *J. Mater. Chem.* **9**, 1347 (1999).
30. Leglise, J., Van Gestel, J., and Duchet, J. C., *J. Chem. Soc. Chem. Commun.* 611 (1994).
31. Wambeke, A., Jalowiecki, L., Kasztelan, S., Grimblot, J., and Bonnelle, J. P., *J. Catal.* **109**, 320 (1988).
32. Reinhoudt, H. R., Boons, C. H. M., Van Langeveld, A. D., Van Veen, J. A. R., Sie, S. T., and Moulijn, J. A., *Appl. Catal. A* **207**, 25 (2001).
33. Sauer, N. N., Markel, E. J., Schrader, G. L., and Angelici, R. J., *J. Catal.* **117**, 295 (1989).
34. Broderick, D. H., Sapre, A. V., Gates, B. C., Kwart, H., and Schuit, G. C. A., *J. Catal.* **73**, 45 (1982).
35. Rauchfuss, T. B., *Prog. Inorg. Chem.* **39**, 259 (1991).
36. Angelici, R. J., *Bull. Soc. Chim. Belg.* **104**, 265 (1995).
37. Robinson, W. R. A. M., Van Veen, J. A. R., De Beer, V. H. J., and Van Santen, R. A., *Fuel Proc. Techn.* **6**, 89 (1999).